Carbon 130 (2018) 19–24

Contents lists available at ScienceDirect

Carbon

journal homepage: www.elsevier.com/locate/carbon

Passivation of hydrogen damage using graphene coating on α-Fe_2O_3 films

Li Chen [a, *], Changmin Shi [a], Xiaolong Li [a], Zhishan Mi [b], Chuan Jiang [c], Lijie Qiao [b, **], Alex A. Volinsky [d]

[a] Institute of Condensed Matter Physics, Linyi University, Shandong 276000, People's Republic of China
[b] Corrosion and Protection Center, Key Laboratory for Environmental Fracture (MOE), University of Science and Technology Beijing, Beijing 100083, People's Republic of China
[c] Department of Data Acquisition, National Instruments, Austin, TX 78759-3504, USA
[d] Department of Mechanical Engineering, University of South Florida, Tampa, FL 33620, USA

ARTICLE INFO

Article history:
Available online 29 December 2017

ABSTRACT

We report the demonstration of graphene as a passive layer that prevents hydrogen damage of steels. The effectiveness of the hydrogen damage inhibition is evaluated using graphene on α-Fe_2O_3 films. It's been observed that the work function increases under both compressive and tensile strains compared with α-Fe_2O_3 films without graphene coating, which indicates that the graphene coating strained surface layer became more corrosion resistant. The investigation of strain effect on the work function would help fundamentally understand the corrosion behavior. Our findings confirm that the graphene coating is an effective means to inhibit corrosion, even on deformed steels.

1. Introduction

The effect of hydrogen on steels is known as hydrogen embrittlement (HE) [1]. Hydrogen dissolved in metals significantly affects composition, structure and mechanical properties of passive films. For example, hydrogen can induce low yield and fracture stresses in steels [2–6]. In order to protect steels from hydrogen permeation and prevent HE, many approached have been developed, including polyaniline nanofibers [7], heat treatment [8], neon/helium glow discharge [9] and inhibitors of hydrogen permeation [10]. Carbon steel surface can form a passive layer, which is composed of α-Fe_2O_3 [7]. Although stainless steel is better resisting corrosion than other metals, it can be susceptible to localized forms of corrosion attack, which can result in pitting and cracking [11]. It is reasonable to expect that coatings can result in better corrosion resistant materials, while improving surface properties or interfaces with the surrounding media [12].

It is known that graphene is highly stable at ambient atmosphere, up to 400 °C [13]. Controlled formation of graphene-grade coatings in the form of single sheets with homogeneously distributed 2–4 μm long nano-pillars across porous stainless steel substrates was demonstrated by scanning electron microscopy (SEM) [11]. These layers act as a protective coating, inhibiting corrosion and oxidation of the underlying metal [11,14–18]. The presence of the graphene highly enhances steel corrosion resistance and electrical conductivity without altering its other properties. Hydrogen chemisorption on graphene has been shown to form sp^3 hybrdization [19,20], which enables graphene stability for hydrogen storage [21,22]. There are related research reports focused on the elastic constants and the mass of a single graphene layer by applying a pressure difference [23]. Ni-graphene coatings were fabricated by reverse pulse electrodeposition and were more effective in protecting quenching and partitioning steel substrate from HE [24,25]. However, current understanding of graphene on α-Fe_2O_3 as a protective barrier against hydrogen damage is still somewhat limited, which has motivated the present study. More specifically, atomic structure of Fe oxide films controls its protective properties, where interfacial strain due to lattice mismatch and charge transfer due to chemical heterogeneity between the Fe oxide film and steel are unavoidable. Thus, strain and charge transfer are two important extrinsic factors to alter intrinsic properties of ultrathin Fe oxide films grown on steels. Protective properties of graphene coating on α-Fe_2O_3 films have also been investigated coupled with applied stress and hydrogen.

* Corresponding author.
** Corresponding author.
E-mail addresses: chenli@lyu.edu.cn (L. Chen), lqiao@ustb.edu.cn (L. Qiao).

https://doi.org/10.1016/j.carbon.2017.12.119
0008-6223/

Using first-principles calculations, this paper demonstrates that hydrogen damage can be inhibited in graphite-coated α-Fe_2O_3 films. Since graphite films are readily available, we propose that graphite can be used as a better corrosion resistant material than graphene to circumvent the difficulties associated with graphene synthesis for certain applications. These calculation results allow concluding that the work function of α-Fe_2O_3 films can be modified by graphene (graphite) coatings on α-Fe_2O_3 films, which is significantly useful for passivation of hydrogen damage. Future experimental studies will demonstrate its advantages for the coatings industry.

2. Methods and parameters

The electronic structure and properties were calculated as reported earlier [26–28] in the framework of the Vosko-Wilk-Nusair local density approximation LDA + U using Vienna ab initio simulation package (VASP) package. All calculations were performed with a plane-wave cutoff of 400 eV on a 5 × 5 × 1 Monkhorst-Pack k-point mesh. It is strictly required to increase LMAXMIX to 4 (d elements). For structural relaxation, all the atoms are allowed to relax until atomic forces are smaller than 0.01 eV/Å. The optimized lattice constant for the 1 × 1 × 1 Fe terminated α-Fe_2O_3 thin film is $a = 5.014$ Å, which is in agreement with experimentally derived structural parameter 5.035 Å [29]. In our study we used $a = 5.035$ Å. Our tested calculations confirm that U = 5 eV provides a good description of the band gap and magnetic moment of Fe compared with experimental one [30]. The polar (0001) surface has been modeled by containing 1 hexagonal unit cell layer (eighteen atomic layers) for the α-Fe_2O_3 and 1 to 4 graphene layers, and a 1 × 1 periodicity in the surface, containing 30 to 63 atoms (with H adsorbed 4 layer graphene), respectively. There is one H atom absorbed on Fe_2O_3 and graphene coated Fe_2O_3 in a unit cell. The adsorption energies are −1.0718eV, −1.5888eV, and −1.1558eV for graphene absorbed on Fe_2O_3, H atom absorbed on Fe_2O_3, H atom absorbed on graphene, respectively. The adsorption energies are negative, indicating that the adsorption systems are all thermodynamically stable. The use of symmetric slabs cancels out the dipole moments, which can occur in nonsymmetric slabs. The vacuum layer is about 15 Å thick for the system with strain up to ±6% (+for tensile strain, - for compressive strain).

3. Results and discussion

In order to study how hydrogen damage could be inhibited in Fe_2O_3 with graphene coating, one should start from the system without H damage and graphene coating. Fig. 1(a) for the spin-up and 1(b) for the spin-down show typical band structures of p_x, p_y, and p_z states for the free standing Fe terminated α-Fe_2O_3 1 × 1 × 1 with 1.31 nm thickness corresponding cell of 30 atoms in eighteen atomic layers, which reflect the main p_x, p_y, and p_z states of O atoms below E_F. Fe 3d (d_{xy}, d_{yz}, d_{z2}, d_{xz} and d_{x2}) states are more pronounced above E_F, as seen from Fig. 1(c) for the spin-up and 1(d) for the spin-down. The conduction band minimum (CBM) is mainly populated by the unoccupied dz^2 levels of Fe. Although there is some admixture of O-p states throughout both the filled and unfilled bands, the about 90% contribution to valence band comes from oxygen p states, while the occupied 3d levels of Fe lie around 6–7 eV below the Fermi level and at 0–3 eV below the Fermi level dominated by O 2p states is more pronounced. This is a consequence of the fact that the on-site Coulomb potential acts only on the Fe 3d states, leading to a reduction of the Fe-O hybridization which is too strong. It can be seen that it is a charge transfer type of insulator with 1.783 eV band gap rather than a Mott-Hubbard insulator. For H adsorption the bridge site just about top of O

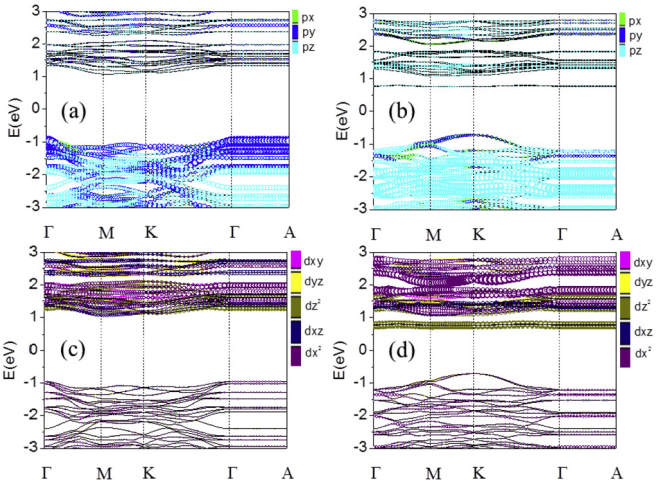

Fig. 1. Band structures along the Γ- M- K- Γ- A directions of Fe_2O_3 film without H adsorption, the p_x, p_y, and p_z states with (a) spin-up and (b) spin-down; the d_{xy}, d_{yz}, d_{z2}, d_{xz} and d_{x2} states with (c) spin-up and (d) spin-down, respectively. Green, blue, cyan, magenta, yellow, dark yellow, navy, purple lines on the bands illustrate the contribution from p_x, p_y, p_z, d_{xy}, d_{yz}, d_{z2}, d_{xz} and d_{x2} states. (A colour version of this figure can be viewed online.)

atom for H adsorption is energetically favored by comparing the relative stability of hollow and top sites of Fe atomic layer. The bond length between H and O atoms attached with the adatoms is 0.979 Å. Fig. 2(a) and (b) present the bands with spin-up and down, which reflect main p_x, p_y, and p_z states of O atoms below E_F, respectively. Fig. 2(c) and (d) present the bands with spin-up and down for d states, respectively. With H adsorption, the p_x states on valence band are enhanced and the CBM is mainly populated by the unoccupied d_{xy} levels of Fe. The increased surface coupling continues to further split and reshape the bands. Almost even bands showing spin split slightly along K- Γ line of band structure, are just below E_F. In this case, the CBM becomes more dispersive than that of the pristine α-Fe_2O_3, indicating that H adsorbed α-Fe_2O_3 thin film may reduce the effective mass for electrons. In H adsorbed α-Fe_2O_3 thin film there is one electrons transfer from H to O, which results

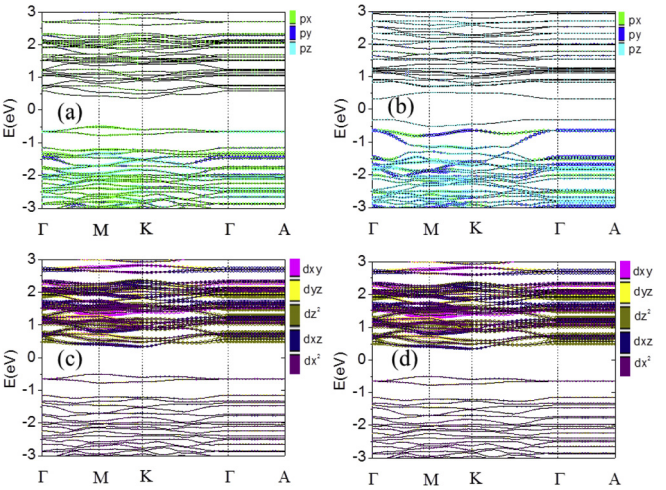

Fig. 2. Band structures along the Γ- M- K- Γ- A directions of Fe_2O_3 film with H adsorption, the p_x, p_y, and p_z states with (a) spin-up and (b) spin-down; the d_{xy}, d_{yz}, d_{z2}, d_{xz} and d_{x2} states with (c) spin-up and (d) spin-down, respectively. Green, blue, cyan, magenta, yellow, dark yellow, navy, purple lines on the bands illustrate the contribution from p_x, p_y, p_z, d_{xy}, d_{yz}, d_{z2}, d_{xz} and d_{x2} states. (A colour version of this figure can be viewed online.)

in band gap decreasing. A short analysis of the band structure features indicates that the presence of H leads to a reduction in the band gap width by approximately 0.8 eV. When H adsorbs onto an O atom, it effectively breaks the bonding between the adsorbed O and its Fe neighbors, which gives rise to flat bands of edge states below E_F, same as H adsorbs on grephene [19]. Consequently, the resulting magnetism is the same as the edge magnetism produced by H on the surface. These results confirm that hydrogen changes the properties of α-Fe_2O_3 films.

Four sites, top (T), bridge (B), hollow (H) and arbitrary non-symmetric sites with blue circles guiding our eyes in Fig. 3(a)–(d), are considered for the relative sites between Fe and C atoms in intrinsic graphene. The C, Fe and O atoms are shown as grey, brown and red balls, respectively. The graphene layer is on the top with hexagon dash line and the Fe_2O_3 slab is below the graphene layer. We found that energetically the most favorable site is T site for C atoms on the top of Fe atoms with interfacial distance of 3.134 Å, which is noticeably typical value of the van der Waals bond. In graphene, each carbon atom is bonded with three neighboring carbon atoms in sp^2 hybridization, leaving one electron in the p_z orbital. For H chemisorption, the most stable configuration is for H atom to bond on top of a carbon atom forming an sp^3 hybrdization [19,31,32]. It is above 2.89 eV of energy barrier that H atom passes through a center of hexagonal structure in graphene because of a repulsive force induced by strong electron cloud of graphene [33,34], which is much larger than the energy barrier of C-H forming (0.18 eV) [35]. Therefore, hydrogen penetration through graphene is much harder than C-H sp^3 formation. This theoretical calculation confirms that charged hydrogen is combined with graphene as C-H bonds, which stops hydrogen penetration into the Fe_2O_3 film. We should study if the presence of the graphene alters the system properties. Fig. 4(a) for spin-up and (b) for spin-down present the band structures of p_x, p_y, and p_z states, and Fig. 4(c) for spin-up and (d) for spin-down present the band structures of d_{xy}, d_{yz}, d_{z2}, d_{xz} and d_{x2} states long the Γ- M- K- Γ- A directions of graphene coated Fe_2O_3 film, respectively. Except three graphene bands in the band gap (~1.7 eV) of the α-Fe_2O_3 films, there

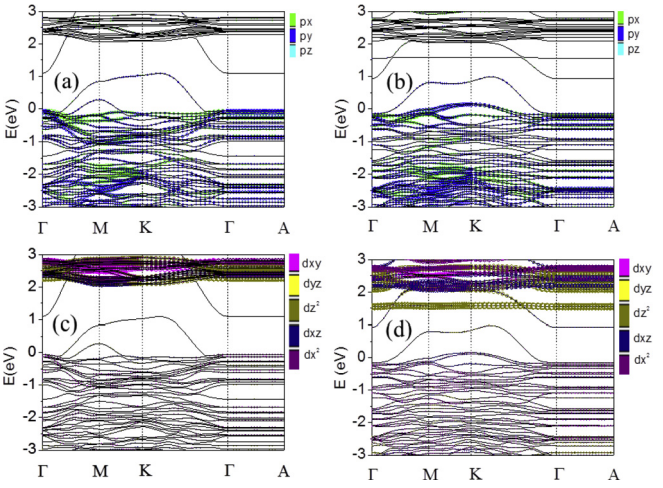

Fig. 4. Band structures along the Γ- M- K- Γ- A directions of graphene coated Fe_2O_3 film with H adsorption, the p_x, p_y, p_z state with (a) spin-up and (b) spin-down, and the d_{xy}, d_{yz}, d_{z2}, d_{xz} and d_{x2} states mainly from Fe atoms with (c) spin-up and (b) spin-down, respectively. Green, blue, cyan, magenta, yellow, dark yellow, navy, purple lines on the bands illustrate the contribution from p_x, p_y, p_z, d_{xy}, d_{yz}, d_{z2}, d_{xz} and d_{x2} states. (A colour version of this figure can be viewed online.)

is almost no change in the features of the CBM because it still has Fe 3d character and valence band because it still has O 2p character. There are still main p_x, p_y, and p_z states of O atoms below E_F. and Fe 3d (d_{xy}, d_{yz}, d_{z2}, d_{xz} and d_{x2}) states are more pronounced above E_F. The CBM is still mainly populated by the unoccupied d_{z2} levels of Fe. Without graphene coating, H adsorption on α-Fe_2O_3 film alters the electronic structure of the system, while the presence of graphene does not alter the system properties, except for electrical conductivity and work function.

The work function (W) is calculated as the difference between the vacuum level E_{vacuum} and the Fermi energy E_F:

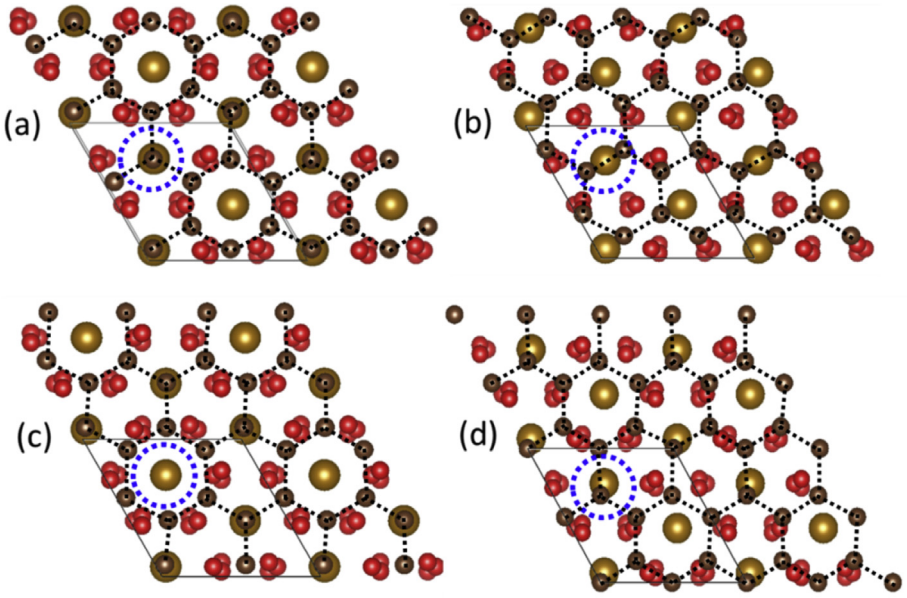

Fig. 3. Relative sites between Fe atoms in top layer of Fe_2O_3 and C atoms in intrinsic graphene with blue circles guiding our eyes. C, Fe and O atoms are shown as gray, brown and red balls, respectively. (a) top (T) site, C atom on the top of Fe atom; (b) bridge (B) site, Fe atom at the bridge of C-C bond; (c) hollow(H) site, Fe atom at the hollow of hexagonal C atoms; (d) arbitrary non-symmetric site. The rhombus shows the unit cell. The graphene layer is on the top with hexagon dash lines and the Fe_2O_3 slab is below the graphene layer. (A colour version of this figure can be viewed online.)

$$W = E_{vacuum} - E_F \quad (1)$$

Here, W reflects electronic energy level so it is related to its electrostatic potential. Based on experimental observations and theoretical studies, we know that the work function is closely related to the corrosion potential. The lower the work function of the material, the easier corrosion occurs, i.e. the work function is a sensitive parameter for the corrosion behavior [36]. The work function of clean Fe_2O_3 is 5.62 eV. The W is shown in Fig. 5(a) for H adsorbed on Fe_2O_3 with and without the graphene coating. It is 4.924 eV for H adsorbed Fe_2O_3 film without the graphene coating. It is indispensable to understand why the presence of H adsorption can decrease the work function of surfaces. The mathematical expression for the work function change can be approximated by the Helmholtz equation [37],

$$\Delta W = q_e n_s \Delta P_z / \varepsilon_0 \quad (2)$$

where q_e is the elemental charge, ε_0 is the electrical permeability in vacuum, n_s is the concentration of adsorbates at the surface, which leads to the changes in the surface dipole, and ΔP_z is the normal component of the dipole moment changes. ΔP_z is given as: [37]

$$\Delta P_z = \int_{z_0}^{z} z\, \Delta\rho(z) dz \quad (3)$$

where z is the coordinate perpendicular to the surface plane, $\Delta\rho$ is the electronic charge density difference at z. With this definition, a positive value of $\Delta\rho$ indicates a dipole oriented to the film side, and its presence produces a decrease of the work function relative to the upper surface. W is 5.55 eV for graphene/Fe_2O_3 film with H adsorption, which is larger than for H adsorbed on the Fe_2O_3 film without graphene coating. H adsorption on Fe_2O_3 film without graphene coating decreases the W about 16.8%, while the change of W only is about 6.3% for H adsorption on graphene/Fe_2O_3 film. W is closely related to the corrosion potential and is a sensitive parameter for corrosion behavior. Our results suggest that the corrosion potential increases and hydrogen damage could be inhibited using graphene coating on the α-Fe_2O_3 films. Unfortunately, the protective efficiency of the monolayer graphene is not perfect. Despite the promise shown by theoretical studies of this system, experimental realization remains challenging because synthesis of graphene is a difficult task. Since graphite film is readily available, we propose that graphite may be used as a better candidate of hydrogen damage inhibition to circumvent difficulties associated with the graphene synthesis for certain applications. We modeled H adsorbed graphite films on α-Fe_2O_3 films for inhibition of hydrogen damage. It is expected that the efficiency can be enhanced with multiple layers of graphene. From our results, W is 5.64 eV and 5.69 eV for two and four layers graphene/Fe_2O_3 film with H adsorption, respectively. Graphite presence is shown to enhance resistance to hydrogen damage. Therefore, because graphite film is readily available, we propose that for corrosion inhibition applications graphite can indeed be used as a better candidate of inhibition of hydrogen damage than graphene.

There could be different factors, such as epitaxial strain, structural deformation, molecular orbital hybridization, and interfacial charge transfer, affecting corrosion properties of α-Fe_2O_3 films. However, experimental and theoretical analyses suggest that strain and H damage on the α-Fe_2O_3 films are most dominating [38–40]. Next, we discuss and compare the work function associated with the H adsorption in the strained system. Fig. 5(b) depicts the work function as a function of strain in different systems with H

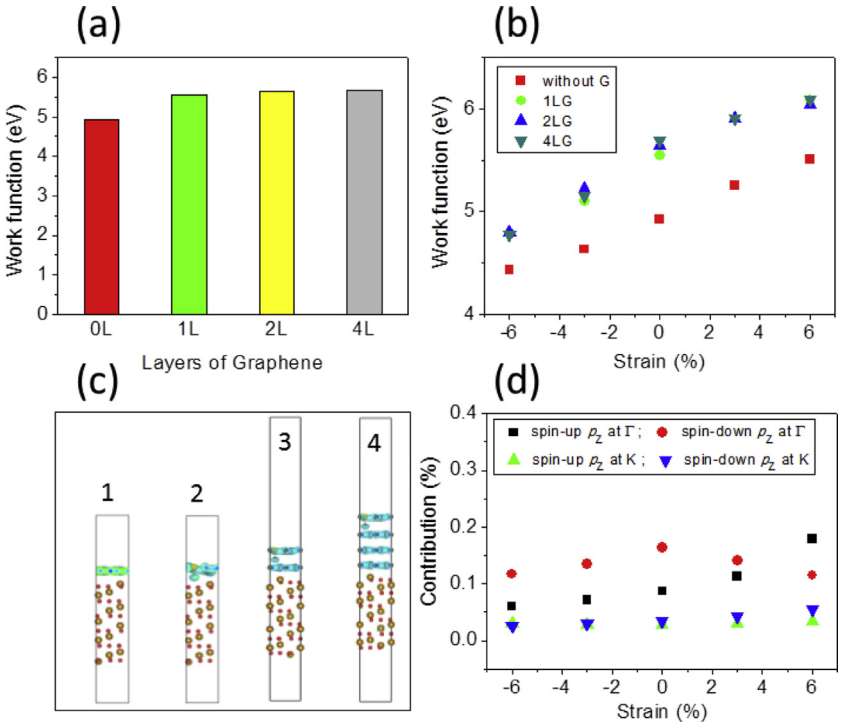

Fig. 5. (a) The work function of H adsorption on Fe_2O_3 film, 1L graphene/Fe_2O_3 film, 2L graphene/Fe_2O_3 film and 4L graphene/Fe_2O_3 film, marked in red, green, yellow and grey colors, respectively. (b) The work function as a function of strain in four systems of (a), marked in red, green, blue and dark cyan colors, respectively. Interfacial charge transfer (c) 1–2, corresponding to one graphene layer on a unit Fe_2O_3 film with and without H adsorption, respectively, (c) 3–4, corresponding two and four graphene layers on a unit Fe_2O_3 film with H adsorption, respectively, The charge density isosurface is set to be 0.12 e/Å^3. (d) The spin polarized p_z state change with increasing strain at K and Γ points in valence band for graphene/Fe_2O_3 with H adsorption. (A colour version of this figure can be viewed online.)

adsorption. The W for without graphene coating system dramatically decreases under compressive strain up to −6%, while it significantly increases under tensile strain up to 6%. For example, it is 4.633 eV under −3% strain with $a = 4.884$ Å and 4.433 eV under −6% strain with $a = 4.733$ Å, respectively, while it is 5.256 eV under 3% with $a = 5.186$ Å and 5.511 eV under 6% strain with $a = 5.337$ Å. This happens because external compressive (tensile) stress may further decrease (increase) the electrostatic potential and thus, leads to the Fermi level change and further decrease (increase) in W. W for graphene coating system obviously increases both under compressive and tensile strain. The relationship between strain and electrostatic potential (or corrosion potential) has not been established in previous theoretical studies. According to previous studies of deformation effects on metal electron gas, it is possible to qualitatively predict changes in the electrode potential [41] and hence estimate the effect of deformation on the corrosion potential. Experimental data showed a rather complicated relationship between the stress and corrosion parameters [42]. With increasing number of graphene layer in Fig. 5(b), W for 2L and 4L graphene coating system increases slightly, compared with that of graphene coating system. The presence of graphene (graphite) could highly enhance corrosion resistance of the system under compressive and tensile strain. The possibility of α-Fe_2O_3 H damage is prevented under strain due to the presence of graphene (graphite) protective coating.

It is essential to understand the mechanism of graphene (graphite) protective coating. Differential charge density at the surface is defined as:

$$\rho = \rho_{H/graphene/Fe2O3} - \rho_{H/graphene} - \rho_{Fe2O3} \quad (4)$$

where $\rho_{H/graphene/Fe2O3}$ is the total charge density, $\rho_{H/graphene}$ and ρ_{Fe2O3} is the charge density of H/graphene and Fe_2O_3 at the same surface lattice constant. The charge transfer was not found between graphene (graphite) and the Fe_2O_3 layers, which confirmed weak coupling at the interface seen in Fig. 5(c). Clearly, the charge transfer is only shown between H and graphene (graphite). The p_z state with spin up and down at the K point in the valence band (seen from Fig. 4(a–b)) is insensitive to strain. This implies the surface state arising from the states of graphene, while the bulk band, with spin up and down at the Γ point, arising from extended Bloch states of Fe_2O_3, is sensitive to strain, as seen from Fig. 5(d) because the strain changes interface spacing and coupling. Regardless of the contribution coming from the p_z states with spin-down decreases under tensile strain, the total contribution of the p_z states, including spin up and down still increases. The contribution coming from the p_z state is larger than of the Fe_2O_3 films without graphene, no matter with or without strain. The electrons of the p_z state have relatively small momentum because the interlayer conduction along the z-direction is severely suppressed based on a very flat conduction band between Γ and A in Fig. 4. With the increase of the p_z state contribution, the amount of electrons with less momentum increases, so that total momentum decreases, and then the total wave vector and the Fermi sphere radius decrease with the corresponding Fermi energy decreasing. Therefore, W ($E_{vacuum} - E_F$) increases compared with α-Fe_2O_3 thin films without the graphene coating. Consequently, increasing W results in better corrosion resistance, allowing to improve surface properties along with interfaces with the surrounding media.

4. Conclusions

In conclusion, a study of graphene as a protective barrier against H damage was carried out. Through the characterization of hydrogen adsorbed graphene, it was identified that graphene can effectively protect hydrogen penetration by the formation of C-H bonds. Calculations show that graphene is a proper barrier for hydrogen penetration and can effectively avoid H damage mentioned by previous research work [4]. It is reasonable to consider that graphene is a more corrosion resistant material, which can improve surface properties and the interface with the surrounding medium. Although inch-sized single-crystalline graphene from a controlled single nucleus on Cu–Ni alloys have grown, but there is still a big challenge in the production high quality graphene at low cost and in large scale [43,44]. Since graphite film is already available, while mass production of graphene remains difficult, we argue that graphite can be superior for protective applications compared with graphene.

Notes

The authors declare no competing financial interest.

Acknowledgments

The work is supported by the National Natural Science Foundation of China (Grants 51431004 and 11634007).

References

[1] W.H. Johnson, On some remarkable changes produced in iron and steels by the action of hydrogen acids, Proc. Roy. Soc. Lond. 23 (1874) 168–179.
[2] Y. Mine, K. Hirashita, M. Matsuda, M. Otsu, K. Takashima, Effect of hydrogen on tensile behaviour of micrometre-sized specimen fabricated from a metastable austenitic stainless steel, Corrosion Sci. 53 (2011) 529–533.
[3] M. Wang, E. Akiyama, K. Tsuzaki, Effect of hydrogen on the fracture behavior of high strength steel during slow strain rate test, Corrosion Sci. 49 (2007) 4081–4097.
[4] Y. Yao, L.J. Qiao, A.A. Volinsky, Hydrogen effects on stainless steel passive film fracture studied by nanoindentation, Corrosion Sci. 53 (2011) 2679–2683.
[5] T. Zakroczymski, A. Glowacka, W. Swiatnicki, Effect of hydrogen concentration on the embrittlement of a duplex stainless steel, Corrosion Sci. 47 (2005) 1403–1414.
[6] D. Hardie, E.A. Charles, A.H. Lopez, Hydrogen embrittlement of high strength pipeline steels, Corrosion Sci. 48 (2006) 4378–4385.
[7] B. Yao, G.C. Wang, J.K. Ye, X.W. Li, Corrosion inhibition of carbon steel by polyaniline Nanofibers, Mater. Lett. 62 (2008) 1775–1778.
[8] S.J. Kim, H.G. Jung, K.Y. Kim, Effect of post-weld heat treatment on hydrogen-assisted cracking behavior of high-strength process pipe steel in a sour environment, Scr. Met. 67 (2012) 895–898.
[9] Y. Yamauchi, K. Takeda, Y. Nobuta, T. Hino, Hydrogen and helium removal retained in stainless steel by neon glow discharge, J. Nucl. Mater. 390–391 (2009) 1048–1050.
[10] M. Elboujdaîni, V.S. Sastri, J.R. Perumareddi, Studies on inhibition of hydrogen-induced cracking of linepipe steels, Corrosion 62 (2006) 29–34.
[11] L.F. Dumée, L. He, Z.Y. Wang, P. Sheath, J.Y. Xiong, C.F. Feng, et al., Growth of nano-textured graphene coatings across highly porous stainless steel supports towards corrosion resistant coatings, Carbon 87 (2015) 395–408.
[12] D. Figueroa, M.J. Robinson, The effects of sacrificial coatings on hydrogen embrittlement and re-embrittlement of ultra high strength steels, Corrosion Sci. 50 (2008) 1066–1079.
[13] L. Liu, S. Ryu, M.R. Tomasik, E. Stolyarova, N. Jung, M.S. Hybertsen, M.L. Steigerwald, Graphene oxidation: thickness-dependent etching and strong chemical doping, Nano Lett. 8 (2008) 1965–1970.
[14] D. Prasai, J.C. Tuberquia, R.R. Harl, G.K. Jennings, K.I. Bolotin, Graphene: corrosion-inhibiting coating, ACS Nano 6 (2012) 1102–1108.
[15] N.T. Kirkland, T. Schiller, N. Medhekar, Exploring graphene as a corrosion protection barrier, Corrosion Sci. 56 (2012) 1–4.
[16] G.E. Haslam, X.Y. Chin, G.T. Burstein, X-ray photoelectron spectroscopy of the passive surface of nickel-carbon electrocatalysts after polarisation in sulfuric acid, Electrochim. Acta 118 (2014) 157–162.
[17] G.E. Haslam, X.Y. Chin, G.T. Burstein, Passivity and electrocatalysis of nano-structured nickel encapsulated in carbon, Phys. Chem. Chem. Phys. 13 (2011) 12968–12974.
[18] S.S. Chen, L. Brown, M. Levendorf, W.W. Cai, S.Y. Ju, J. Edgeworth, et al., Oxidation resistance of graphene-coated Cu and Cu/Ni alloy, ACS Nano 5 (2011) 1321–1327.
[19] L. Chen, H. Hu, Y. Ouyang, H.Z. Pan, Y.Y. Sun, F. Liu, Atomic chemisorption on graphene with stone–thrower–wales defects, Carbon 49 (2011) 3356–3361.
[20] L. Chen, Y. Ouyang, Y.L. Wang, Y.Y. Sun, H.Z. Pan, Hongzhe Pan, The influence of Stone–Wales defects on magnetic properties in graphene, Phys. E 43 (2010) 593–597.

[21] V. Tozzini, V. Pellegrini, Reversible hydrogen storage by controlled buckling of graphene layers, J. Phys. Chem. C 115 (2011) 25523–25528.
[22] V. Tozzini, V. Pellegrini, Prospects for hydrogen storage in graphene, Phys. Chem. Chem. Phys. 15 (2013) 80–89.
[23] J.S. Bunch, S.S. Verbridge, J.S. Alden, A.M. Van der Zande, J.M. Parpia, H.G. Craighead, et al., Impereable atomic membranes from graphene sheets, Nano Lett. 8 (2008) 2458–2462.
[24] P.W. Zhou, W. Li, X. Zhu, Y. Li, X.J. Jin, J. Chen, Graphene containing composite coatings as a protective coatings against hydrogen embrittlement in quenching & partitioning high strength steel, J. Electrochem. Soc. 163 (2016) D160–D166.
[25] T.H. Nam, J.H. Lee, S.R. Choi, J.B. Yoo, J.G. Kim, Graphene coating as a protective barrier against hydrogen embrittlement, Int. J. Hydrogen Energy 39 (2014) 11810–11817.
[26] L. Chen, D.C. Yu, F. Liu, Magnetism in nanopatterned graphite film, Appl. Phys. Lett. 93 (2008), 223106(1) –3).
[27] Z.F. Wang, L. Chen, F. Liu, Tuning topological edge states of Bi(111) bilayer film by edge adsorption, Nano Lett. 14 (2014) 2879–2883.
[28] L. Chen, Z.F. Wang, F. Liu, Robustness of two-dimensional topological insulator states in bilayer bismuth against strain and electrical field, Phys. Rev. B 87 (2013), 235420(1) –5).
[29] L.W. Finger, R.M. Hazen, Crystal structure and isothermal compression of Fe_2O_3, Cr_2O_3, and V_2O_3 to 50 kbars. Locality: synthetic, J. Appl. Phys. 51 (1980) 5362–5367.
[30] S. Mochizuki, Electrical conductivity of alpha-Fe_2O_3, Phys. Status Solidi 41 (1977) 591–594.
[31] D.C. Yu, F. Liu, Synthesis of carbon nanotubes by rolling up patterned graphene nanoribbons using selective atomic adsorption, Nano Lett. 7 (2007) 3046–3050.
[32] Z.F. Wang, Y. Zhang, F. Liu, Formation of hydrogenated graphene nanoripples by strain engineering and directed surface self-assembly, Phys. Rev. B 83 (2011), 041403(R) (1)–4).
[33] M. Miao, M.B. Nardelli, Q. Wang, Y. Liu, First principles study of the permeability of graphene to hydrogen atoms, Phys. Chem. Chem. Phys. 15 (2013) 16132–16137.
[34] Y.S. Nechaev, T.N. Veziroglu, Thermodynamic aspects of the graphene/graphane/hydrogen systems: relevance to the hydrogen on-board storage problem, Adv. Mater. Phys. Chem. 3 (2013) 255–280.
[35] Y. Miura, H. Kasai, W.A. Dino, H. Nakanishi, T. Sugimoto, Effective pathway for hydrogen atom adsorption on graphene, J. Phys. Soc. Jpn. 72 (2003) 995–997.
[36] H. Luo, C.F. Dong, Characterization of passive film on 2205 duplex stainless steel in sodium thiosulphate solution, Appl. Surf. Sci. 258 (2011) 631–639.
[37] M.F. Juárez, e Santos, Electronic anisotropy at vicinal Ag(11n) surfaces: work function changes induced by steps and hydrogen adsorption, J. Phys. Chem. C 117 (2013) 4606–4618.
[38] O.M. Alyousif, R. Nishimura, Stress corrosion cracking and hydrogen embrittlement of sensitized austenitic stainless steels in boiling saturated magnesium chloride solutions, Corrosion Sci. 50 (2008) 2353–2359.
[39] L.J. Qiao, W.Y. Chu, H.J. Miao, J.M. Xiao, P.X. Guo, Hydrogen-facilitated corrosion and stress corrosion cracking of austenitic stainless steel of type 310, Metall. Trans. A 24A (1993) 959–961.
[40] W.W. Wang, Y.J. Su, Y. Yan, J.X. Li, L.J. Qiao, W.Y. Chu, et al., The role of hydrogen in stress corrosion cracking of 310 austenitic stainless steel in a boiling $MgCl_2$ solution, Corrosion Sci. 60 (2012) 275–279.
[41] B.I. Kolodii, Theoretical investigation of the interaction of a deformed metal with a corrosion medium, Mater. Sci. 36 (2000) 884–891.
[42] R. Akid, I. Dmytrakh, Influence of surface deformation and electrochemical variables on corrosion and corrosion fatigue crack development, Fatig. Fract. Eng. Mater. Struct. 21 (1998) 903–911.
[43] T. Wu, X. Zhang, Q. Yuan, J. Xue, G. Lu, Z. Liu, et al., Fast growth of inch-sized single-crystalline graphene from a controlled single nucleus on Cu-Ni alloys, Nat. Mater. 15 (1) (2016) 43–47.
[44] Y. Chen, J. Sun, J. Gao, F. Du, Q. Han, Y. Nie, et al., Growing uniform graphene disks and films on molten glass for heating devices and cell culture, Adv. Mater. 27 (2015) 7839–7846.